





Experimental Study of the Charring of I-Joists and Recession of Combustible Insulation in Light Timber Frame Assemblies with Comparison to Eurocode 5

Andreas Sæter Bøe ^{*}, Norwegian University of Science and Technology (NTNU), Trondheim, Norway

Katrin Nele Mäger , Tallinn University of Technology (TalTech), Tallinn, Estonia

Kathinka Leikanger Friquin , SINTEF Research Institute, Trondheim, Norway

Alar Just , Tallinn University of Technology (TalTech), Tallinn, Estonia

Received: 5 November 2021/**Accepted:** 10 July 2023/**Published online:** 31 July 2023

Abstract. Design models are commonly used in fire safety design of light timber frame assemblies. Parameters for use in the models are available for rectangular members with mineral wool, wood fibre or cellulose insulation and for assemblies with I-joists and mineral wool. For assemblies where I-joists and combustible insulations are combined, design parameters are missing. Five fire experiments with two I-joist types and four combustible insulation products have been conducted. The aim was to study charring of I-joist flanges and recession rates of combustible insulations and in addition, to compare their behaviour to the new and existing models of Eurocode 5. Charring rates for the flanges were 0.40–0.76 mm/min and 0.54–1.72 mm/min for the protected and post-protected phase, respectively. Rates decreased with increasing flange size. Charring rates for flanges of solid wood and LVL were comparable. The results show that lateral charring of I-joist flanges can be significant in the protected phase. The tested insulation products showed a lower recession rate than values reported for glass wool insulation, with a more pronounced difference for wood fibre and cellulose insulations. The low recession rates compared to previously reported generic values can possibly be explained by better product-specific properties, negligible shrinking and slightly different test set-up. The insulation stayed well in place after gypsum board fall-off and best-practice for keeping the insulation in place is given. The results, completed with future loaded full-scale tests, can give basis for further development of design models for assemblies with I-joists and combustible insulations.

Keywords: Fire, Fire resistance, Design model, I-joist, Charring rate, Insulation, Degradation rate, Recession rate

^{*}Correspondence should be addressed to: Andreas Sæter Bøe, E-mail: andreas.s.boe@ntnu.no



1. Introduction

Wood has been used extensively in buildings for centuries and the fire performance of traditional structural members has been studied for decades. Simplified design models for predicting char depths and load-bearing capacities for rectangular timber members have been developed earlier.

Design of the fire resistance of timber structures generally consists of two parts: calculation of the charring depth and, thereafter, determination of the mechanical resistance [1–5]. The charring depth is determined based on the charring rate of the wood and will be a function of the wood species, density, moisture, etc. [6, 7].

In fire-resistant design, the primary protection for timber members is offered by claddings. Several methods are developed to determine the residual load-bearing capacity and separating function of timber frame assemblies based on furnace tests with standard fire exposure [8, 9], for example, in Europe [1, 10], USA [2], Canada [5], Australia [11] and New Zealand [11]. The methods are similar, where determination of the char depth is the main principle, but the charring rates vary. In some of the methods, the residual load-bearing capacity for the remaining cross-section will thereafter be determined based on reduced strength and stiffness properties of the wood. In other methods, a layer is deducted from the cross-section due to reduced strength and stiffness properties caused by increased temperature. The residual load-bearing capacity is then determined for the remaining cross-section with strength and stiffness properties at normal temperature. The protection given by claddings or insulation in the cavities is included in different ways. For further comparison, see Buchanan and Östman [12] and LaMalva and Hopkin [3].

In Europe, the methods given in EN 1995-1-2:2004 [1] (EN 1995-1-2) are commonly used for rectangular cross-sections. The main model of EN 1995-1-2 was developed by König and Walleij [13] and considers one-dimensional heat transfer, where the charring rate is treated as a constant. The model transfers the residual cross-section to a rectangular one and accounts for corner rounding by multiplying the one-dimensional charring rate with coefficients.

In the design methods described in EN 1995-1-2 [1], the charring behaviour of the wood is considered in three phases, see Figure 1. In Phase 1, no charring occurs as the cladding protects the timber from direct heat exposure and the temperature on the timber surface has not reached 300°C. Phase 2, also known as the protected phase, begins when the timber has started to char, i.e., the surface of the timber has reached 300°C, but is still protected by the cladding. Phase 3, the post-protected phase, starts when the cladding falls off and the timber members become directly exposed to the fire. To calculate the charring depth of the different phases, additional coefficients for the protected and post-protected phase are added.

For timber frame assemblies with insulated cavities, the charring is also affected by the cavity insulation. A design model for timber members with rectangular cross-sections to include the effect of stone wool insulation in timber frame assemblies is available in Annex C of EN 1995-1-2. Charring is considered to occur only

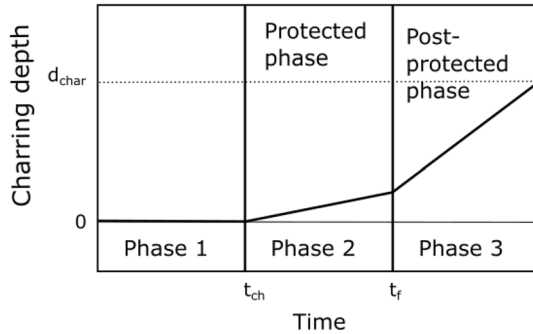


Figure 1. Charring of timber protected by a cladding material. d_{char} represents the final charring depth, while t_{ch} and t_f indicate the start of charring and fall-off of cladding, respectively. Figure based on EN 1995-1-2 [1].

from the fire-exposed side of the cross-section. The lateral sides are considered protected by stone wool. The model is valid also for assemblies with glass wool, but only until fall-off of the cladding.

Improved models that also include glass wool insulation were later developed by Just [14] and published in the handbooks *Brandsäkra trähus* [15] and *Fire safety in timber buildings—Technical Guideline for Europe* [10]. The models are applicable to light timber frame assemblies with rectangular cross-sections of solid timber and cavity insulation of mineral wool. In the COST Action network FP1404 *Fire Safe Use of Bio-Based Building Products* [16], new models were developed based on the previous. Protection levels of insulation were included, protection time of fire protective cladding was improved and the thickness of the zero-strength layer was differentiated for tension, compression and bending in the cross-section. The zero-strength layer is here defined as a layer where the strength and stiffness properties of the wood material are assumed to be zero due to the increased temperatures caused by the fire. This layer is directly behind the charred wood and it is assumed that the strength and stiffness properties of the wood behind the layer are unchanged.

In the last years, the popularity of lightweight engineered wood products has increased. One example is the I-joist, an I-shaped timber member consisting of a top and bottom flange with a web in between. They have become increasingly popular [17], among others, due to their great strength-to-weight ratio. Timber frame assemblies with I-joists are not included in any of the mentioned models [1, 14, 16] and only briefly mentioned in handbooks [10, 15].

König [18] investigated the fire resistance of I-joists and developed models to analyse the load-bearing capacity of I-joists exposed to fire. The assumption for charring calculations was a cavity completely filled with stone or glass wool insulation. Moreover, the model is only valid for glass wool until the failure of the cladding on the fire side.

In addition to new engineered wood products, there is now also a range of different insulation materials available, including combustible insulations. As introduction of combustible insulations might change the fire dynamics of a compartment fire, it is important to understand the contribution of the insulation [19].

The above-mentioned models [1, 10, 14–16, 18] are applicable to assemblies insulated with stone wool and glass wool. Hence, none of the combustible insulation products that have entered the market in the past years, like wood fibre, cellulose and phenolic foam insulations, are included in the models.

However, recently several experiments were carried out on combustible insulations. Tiso [20] conducted 36 furnace tests with a solid wood timber frame and several different cavity insulations. The work resulted in the description of protection levels (PLs) to characterise different insulation materials. The PLs are described in detail later in this section.

Based on the experiments of Tiso [20], Tiso and Just [21–23] developed a design model for timber frame assemblies with rectangular cross-sections and cavities filled with different combustible insulation (wood fibre, cellulose, EPS, PUR and PIR).

Mäger and Just [24, 25] further developed the model of Tiso and Just [21–23] by adding a proposed design model for assemblies with I-joists and mineral wool insulations.

This model includes four different charring phases, see Figure 2. In Phase 1, no charring occurs, while Phase 2 considers charring behind the cladding. Phase 3 is after fall-off of the cladding and an increased charring rate is seen. Phase 3 is followed by Phase 4, which is recognised by a reduced charring rate compared to Phase 3. The reduced charring rate is caused by formation of a sufficiently thick char layer to slow down the heat transport into the char front, approximately 25 mm. Phase 2 is neglected if fall-off of the cladding occurs before charring of the protected wood has started. Similarly, if a sufficiently thick char layer forms in

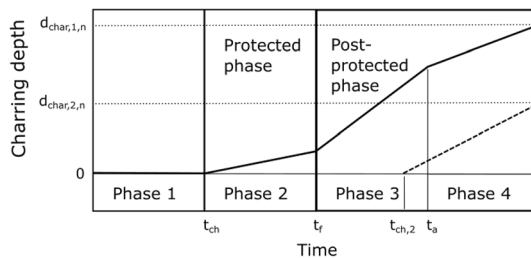


Figure 2. Charring of timber protected by a combustible cavity insulation. t_{ch} and $t_{ch,2}$ represents the start of charring of the exposed and lateral side, respectively. t_r is the time for fall-off of cladding, and t_a is the time when charring is reduced due to a sufficiently thick char layer. $d_{char,1,n}$ and $d_{char,2,n}$ represents the final charring depth for the exposed side and the lateral side, respectively. Figure based on EN 1995-1-2 [1].

Phase 2, Phase 3 is neglected. On the other hand, if the final charring depth does not reach a sufficiently thick layer to reduce charring, Phase 4 is not considered. The start time of charring from the lateral sides may occur in Phase 2, 3 or 4, depending on the insulation properties and the fall-off time for the cladding.

However, design parameters for assemblies of I-joists in combination with combustible cavity insulation have not yet been established. Therefore, predicting the charring of I-joists in these assemblies is not possible based on the currently available design parameters.

A new version of Eurocode 5 is being developed, the final draft of prEN 1995-1-2:2021 [26] (prEN 1995-1-2) is referred to here. It includes a design model for charring of I-joists based on the work of Mäger and Just [24, 25]. The model includes more possibilities for variations of materials and the calculation of the charring depth includes coefficients considering the protection of the timber member, grain direction, thickness, density etc. The design method for I-joists is largely similar to the effective cross-section method (ECSM) [1] for rectangular timber members. The effective cross-section is what remains after the charred material and the layer with reduced strength and stiffness (zero-strength layer) are removed from the timber member.

The prEN 1995-1-2 also provides guidance on how to assess new insulation products based on the work of Tiso [20]. A test method to determine the Protection Levels for insulation products is described. In the test, a small timber frame assembly consisting of solid timber elements with dimensions 45 mm × 145 mm is used. The insulation product is placed in the cavities on each side of the centre beam. The wood frame is closed with a gypsum board on the fire-exposed side and a particleboard on the unexposed side. Thermocouples (TC) are positioned at the intersection between the gypsum board and the wood surface and on the lateral sides of the beams at 100 mm depth. The test specimen is then exposed to the standard fire temperature curve according to EN 1363-1 [27]. The gypsum board is provoked to fall off after 45 min by manual intervention and the test is terminated after 60 min. The Protection Level classification is based on the temperature of the beams at 100 mm depth at 45 and 60 min, with the following classification scheme:

- PL1 if the temperature is lower than 300°C at 60 min.
- PL2 if the temperature is lower than 300°C at 45 min and higher than 300°C at 60 min.
- PL3 if the temperature is higher than 300°C at 45 min.

The recession rate is determined based on the time it takes for the TC at 100 mm depth to reach 300°C. This method presumes that no lateral charring has occurred before fall-off of the gypsum board.

In prEN 1995-1-2, the recession rate for cavity insulation in PL2 made of glass wool is 30 mm/min, based on Just [14]. The rate for wood fibre and cellulose-based insulation in PL2 is 14 mm/min [20]. These values are considered to be on the conservative side.

Winter et al. [28] performed furnace tests of rectangular solid wood members similar to the tests of Tiso [20, 23]. For cellulose insulation, a much lower recession rate was obtained compared to the values of Tiso [20, 23]. The cellulose insulation was classified as PL1 (together with stone wool), while Tiso's measurements put this insulation in PL2 (together with traditional glass wool). Wood fibre insulations were classified as PL2 in both studies [20, 28]. The low recession rates for cellulose insulation were explained by how the insulation was installed, blown-in loose-fill insulation [28] versus manually packed batts [20, 23]. Winter et al. also found large differences in recession rates between insulations installed in a wall configuration compared to a floor configuration.

Although the design model is applicable to I-joists, all known recession rates are derived from tests with solid wood and not I-joists. Hence, design parameters for combustible insulations derived from tests with I-joists are still missing.

To develop a design model for light timber frame assemblies with I-joists and combustible cavity insulation, design parameters for the I-joists and insulation must be determined. The parameters can be determined based on the charring rate of the I-joists on the fire-exposed and lateral sides. The charring on the lateral sides will be influenced by the recession rate of the different types of insulation which, therefore, must be known. The parameters required for calculating the charring depth of the I-joists may be determined by testing, with supplement from thermal finite element simulations. Testing is recommended to gain input for simulations and to verify the results.

The aim of this study was, therefore, to establish the charring rate of I-joists in light timber frame assemblies with combustible cavity insulation. The recession behaviour of different combustible insulation products was also studied. A series of five fire experiments with assemblies with I-joists and combustible insulation was conducted. Two types of I-joists and four different insulation products were used in the experiments.

2. Methods

The experimental method and methods for calculating the charring rates of the I-joists and recession rates of the insulations are described here.

2.1. Experimental Method

2.1.1. Test Specimens In total, five furnace tests were carried out at RISE Fire Research in Trondheim, Norway. The test specimens were built up with various combinations of two different I-joist types and four different insulation products. Details on the I-joists and insulations are given in Sect. 2.1.2 and summarised in Tables 1 and 2. The I-joists were installed in a timber frame. A centre beam divided the frame into two similar-sized rectangular spaces, Space A and B. In each space, three I-joists of the same type but with different flange sizes were installed. The cavities between the I-joists and the frame were completely filled with insulation. The build-up and dimensions are shown in Figure 3. All joints between the solid timber elements in the frame were covered with aluminium tape, see Figure 4

Table 1
Details of the I-Joists Used in the Tests

Name used in the report	Hunton I-joist	Masonite I-joist
Produced by	Steico	Masonite beams
Flange	Laminated veneer lumber—3 mm layer thickness	Solid wood, spruce or pine
Web	8 mm hard fibreboards	10 mm particleboards
Flange height ^a	39 mm	47 mm
Flange width—Small	45 mm	47 mm
Flange width—Medium	60 mm	70 mm
Flange width—Large	90 mm	97 mm

^aThe measured flange height varied slightly between the different I-joists. Hunton: 40–41 mm, Masonite: 47–47.5 mm

Table 2
Insulation Products

Insulation product name	Type	Density	R-value ^a for 200 mm thickness	Material information
CBI isocell evolution	Cellulose fibre, Loose-fill—blown in	~ 57 kg/m ³	5.41 m ² K/W	92% mass weight of unused newspapers, 8% mineral salts without Boron
Hunton Nativo® Wood Fibre	Wood fibre, Loose-fill—manually packed	~ 40 kg/m ³	5.26 m ² K/W	Natural wood fibre from spruce with addition of the fire-retardant ammonium phosphate
Hunton Nativo® Wood Fibre	Wood fibre Batt	~ 51 kg/m ³	5.26 m ² K/W	Natural wood fibre from spruce with addition of the fire-retardant ammonium phosphate
Kingspan Kooltherm K12	Thermoset phenolic Batt	~ 36 kg/m ³	9.52 m ² K/W	Thermoset phenolic foam insulation

^aR-value is insulation thickness [m] divided by the conductivity [W/mK] and is the reciprocal of the U-value

and the joints between the timber elements and the boards were sealed with a fire sealant to reduce smoke and heat leakage during the fire tests.

In Test 1, the same I-joist type was used in both Space A and B, but the cavities in the two spaces were filled with two different insulations. In Tests 2, 3 and 4, the I-joists in Spaces A and B were different, while the insulation was the same type in both spaces. In Test 5, both the I-joist and the insulation were the same in both spaces, but at one side, only the two largest flange sizes were tested. The distance between the I-joists in Test 5 with only two I-joist sizes was 600 mm instead

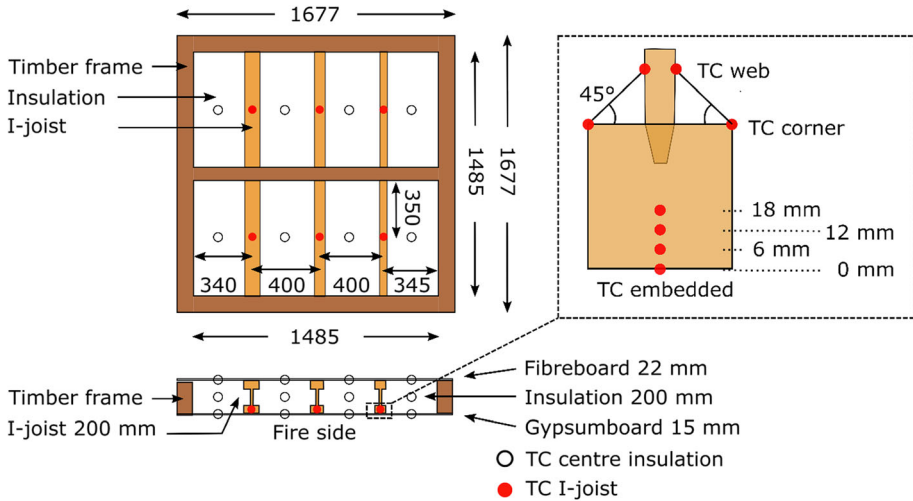


Figure 3. Build-up of test specimen in plan and cross-section, and position of thermocouples. Dimensions in mm.



Figure 4. Left: Test specimen filled with wood fibre batt on the left half side and phenolic foam batt on the right half side. Right: Test specimen filled with wood fibre loose-fill insulation (manually packed) between the Hunton I-joists (left) and Masonite I-joists (right). The fibreboard is not installed.

of 400 mm, which was used in the other tests. The increased centre-centre distance on one side was chosen to study the effect of the insulation width. An overview of all tests is given in Table 3, whereas an explanation for the test ID is given in Figure 5.

The test specimen was protected by a 15.4 mm gypsum board type F, according to the classification of EN 520 [29], on the fire exposed side and covered with a 22 mm fibreboard on the non-exposed side. The screw distance for both the gypsum board and the fibreboard was ca. 300 mm. Each of the two equally sized spaces was completely covered by one separate gypsum board, with no joints on the I-joists or the insulation. The two gypsum boards were cut slightly smaller than the furnace opening, so they could freely fall down into the furnace when the boards or their fasteners failed. The gypsum boards were fastened with 41 mm

Table 3
Test Matrix

TEST ID	Test no	I-joist	Flange width	Insulation
T1MaSKb	1	Masonite (Ma)	S47 mm	Kingspan Kooltherm phenolic foam batt (Kb)
T1MaMKb			M70 mm	
T1MaLKb			L97 mm	
T1MaSHb			S47 mm	Hunton Nativo® Wood Fibre Insulation batt (Hb)
T1MaMHb			M70 mm	
T1MaLHb			L97 mm	
T2HuSClf	2	Hunton (Hu)	S45 mm	CBI Isocell Evolution cellulose (Clf)
T2HuMClf			M60 mm	
T2HuLClf			L90 mm	
T2MaSClf		Masonite (Ma)	S47 mm	
T2MaMClf			M70 mm	
T2MaLClf			L97 mm	
T3HuSHlf	3	Hunton (Hu)	S45 mm	Hunton Nativo® Wood Fibre loose-fill insulation (Hlf)
T3HuMHlf			M60 mm	
T3HuLHlf			L90 mm	
T3MaSHlf		Masonite (Ma)	S47 mm	
T3MaMHlf			M70 mm	
T3MaLHlf			L97 mm	
T4HuSHb	4	Hunton (Hu)	S45 mm	Hunton Nativo® Wood Fibre Insulation batt (Hb)
T4HuMHb			M60 mm	
T4HuLHb			L90 mm	
T4MaSHb		Masonite (Ma)	S47 mm	
T4MaMHb			M70 mm	
T4MaLHb			L97 mm	
T5HuSHb	5	Hunton (Hu)	S45 mm	Hunton Nativo® Wood Fibre Insulation batt (Hb)
T5HuMHb			M60 mm	
T5HuLHb			L90 mm	
T5HuMHbcc60 ^a			M60 mm	
T5HuLHbcc60 ^a			L90 mm	

^aFlange centre-to-centre distance was 600 mm instead of 400 mm

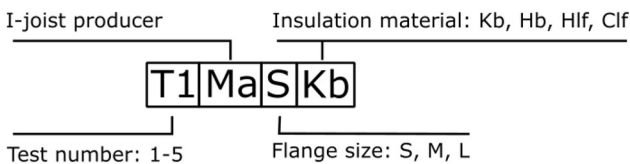


Figure 5. Explanation for the given test IDs.

gypsum screws in Tests 1, 2 and 3, but was reduced to screws with 30 mm length in Test 4 and 5 to reduce the fall-off time.

2.1.2. *I-Joist and Insulation Types* I-joists from two different manufacturers, Masonite and Hunton, were used. They had different materials in the flange and

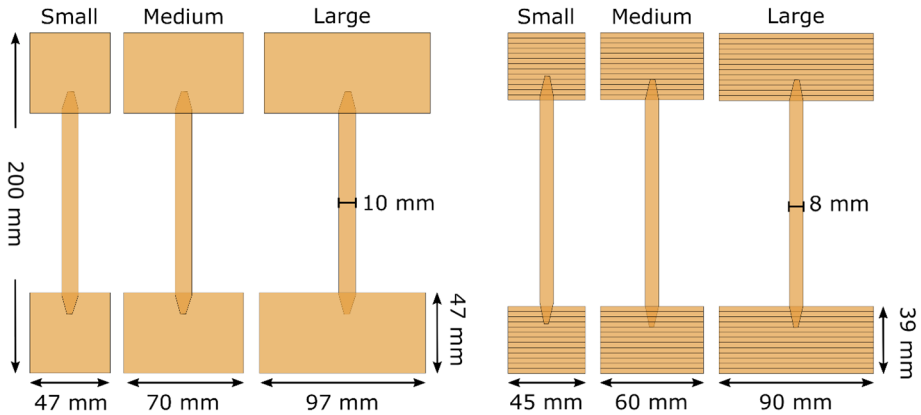


Figure 6. Left: I-joists from Masonite with solid flanges. Right: I-joists from Hunton with LVL flanges.

web and different dimensions, see Figure 6 and Table 1. All tested I-joists had a total depth of 200 mm. The moisture content was measured for all I-joists using a calibrated moisture meter and varied from 11.7% to 13.3%. Two different I-joist products were used as the charring of wood can vary with the wood species, density, moisture or type of engineered timber used in the flange [6].

Four different insulation products were used; Hunton Nativo® Wood Fibre insulation, batt (Hunton batt, wood fibre batt), Hunton Nativo® Wood Fibre insulation, loose-fill (Hunton LF, wood fibre LF), CBI Isocell Evolution insulation of cellulose fibre, loose-fill (Isocell LF, cellulose LF) and Kingspan Kooltherm K12 insulation of thermoset phenolic, batt (phenolic foam batt). See Table 2 for description of the insulation products. The products are produced according to the relevant product standards [30–32].

The wood fibre batts were cut to match the profiles of the I-joists to get an optimised fit. The insulation was cut with a slight overshoot of 15–20 mm to increase the likelihood of the insulation staying in place after the gypsum board fall-off. Due to less elasticity of the phenolic insulation, it was cut to exactly fit the flange-to-flange distance without a profile. The small space between the web and the insulation batts was filled with pieces of phenolic batts as tight as possible. The loose-fill insulation cellulose LF was blown in, while the wood fibre LF was manually packed.

The phenolic insulation consisted of two 100 mm layers. In Tests 1 and 4, the wood fibre batts were 200 mm thick but had to be cut in half (ca. 100 mm) to be installed. In Test 5, 2 × 100 mm thick batts were used.

Except for the blown-in loose-fill insulation, all insulation products were conditioned inside the test hall (ca. 22°C) at least 24 h before installation in the test frame and testing.

2.1.3. Instrumentation The specimens were instrumented with several thermocouples (TC) to measure the temperature development in the assemblies, I-joists and

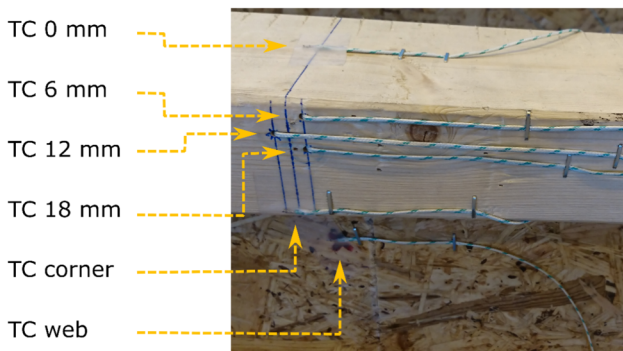


Figure 7. The bottom flanges of the I-joists (fire-exposed side) are instrumented by eight TCs, where six of them are shown in the image. View from the fire exposed side.

insulations. All TCs were of type K (Chromel and Alumel conductors [33]), with an exposed twisted junction of ca. 1.5 mm. Each I-joist was instrumented with eight TCs, see Figures 3 and 7. Four TCs were used to measure the temperature at 0 mm, 6 mm, 12 mm and 18 mm into the bottom flange from the fire exposed side. The embedded TCs were inserted into the side of the flange in 2 mm large holes, drilled in a drill press stand. The depth of the holes reached to the centre of the flange width. In addition, the surface temperature on the top corners of the bottom flange and on the web was monitored. The TCs on the web were attached to the surface by staples and was located at a 45° angle from the corner. The TCs on the corner of the flange were positioned at the top corner of the bottom of the flange, i.e., at 40.5 mm and 47 mm depth for Hunton and Masonite I-joists, respectively. The reason why 40.5 mm was used instead of 39 mm was a small deviation between the measured flange height and the height given by the Hunton I-joist datasheet, see Table 1.

Thermocouples were also installed in the centre between the I-joists. One at the intersection between the gypsum board and insulation, one at the centre of the insulation at 100 mm depth into the insulation and one at the intersection between the fibreboard and the insulation.

All TCs were installed at ~ 350 mm distance from the centre beam and in general, installed to follow the isotherm for at least 50 mm before stretching them from hot to cold temperatures. Stretching them directly from the measurement point to the cold side of the specimen, air gaps around the thermocouples and the thermocouples themselves can lead to errors in the temperature measurements [34–36]. However, in Tests 1–4, the TCs in the centre of the insulation were inserted from the unexposed side of the insulation perpendicular to the predicted isotherms, as no practical method was found to install the TCs parallel to the isotherm. The measurements gave rough indications of temperatures inside the insulation and were only used to support other data. In Test 5, the insulation batts were 2×100 mm thick instead of 1×200 mm and the TCs were, therefore, installed parallel to the isotherm.

2.1.4. Test Procedure The test specimens were mounted horizontally on top of a furnace. The inner dimension of the furnace was 1560 mm × 1560 mm × 1560 mm. The test specimen was aligned symmetrically above the opening with an exposed area of 1560 mm × 1560 mm. The furnace was heated according to the standard time–temperature curve [8, 9]. The aim was to run the tests as long as possible to collect as much data as possible but without a complete charring of the flanges or the web. The tests were planned to be terminated when both the temperature at the web and the flange corner had reached 300°C. However, due to some unforeseen events, like gypsum board failure, insulation fall-down and large temperature differences between the different I-joist sizes, the termination plan was not perfectly followed.

Termination of the test was executed by first turning off the furnace heaters, then cutting the TC wires, lifting the test specimen by a crane and cooling down the test specimen with water from a fire hose. This process lasted about two minutes.

2.1.5. Determination of Residual Height and Cross-Section When the test specimen had cooled down, a sample (~ 50 mm wide) was sawn out of each I-joist close to where the TCs were installed. The char layer of each sample was then physically removed with a steel brush. The remaining height of the I-joist was measured on both sides of the cut sample by a calliper, with an accuracy of 0.5 mm.

To determine the remaining cross-section, the outline of the I-joist samples was drawn on a mm-paper. The remaining area was then calculated using a measurement tool in the vector graphic editing software *Inkscape*, using the mm-paper as reference scale. To verify the calculated area, the remaining height was also calculated and compared with the height measured by the calliper. This method was preferred instead of drawing the outline in a software based on an image because the scaling against a reference turned out to be less accurate.

2.2. Determination of Charring Rates

Two different charring rates have been calculated, before and after fall-off of the gypsum board, i.e., for the protected and post-protected phase.

2.2.1. Protected Phase The charring rate in the protected phase was based on a best-fit regression analysis of the time the embedded TCs reached 300°C before fall-off. The obtained charring rate for this phase was named a1.

In Test 1 with phenolic insulation, the fall-off happened early and the time of start charring happened right after this. Therefore, no protected phase was present with phenolic insulation. In Tests 4 and 5, there was a short protected phase, but not long enough for any of the embedded TCs to reach 300°C. Hence, a charring rate for the protected phase for these tests was not found.

2.2.2. Post-protected Phase The charring rate in the post-protected phase was calculated based on two data points, the charring depth at fall-off of the gypsum board and the final charring depth at the end of test, as explained below:

1. Determination of the charring depth at fall-off of the gypsum board
 - (a) Fall-off time was defined as the time at which the TC-readings at the non-exposed side of the gypsum board made a significant jump and TC readings reached about the same temperature as the furnace.
 - (b) The charring depth at fall-off time was then predicted based on extrapolation of the calculated charring rate before fall-off of the same test. In Tests 4 and 5, the data were insufficient to calculate a charring rate before fall-off and predict the charring depth at fall-off. The charring rate for the same type of insulation from Test 1 was, therefore, used.

The uncertainty of this method was based on how accurate the calculated charring rate before char fall-off was.

2. Determination of charring depth at the end of the test
 - (a) The time for the end of the test was set equal to when the furnace burners were turned off.
 - (b) The charring depth at the end of the test was determined as the difference between the initial height and the measured residual height.

The obtained charring rates for this phase were named a_2 .

The uncertainty of (2a) was related to the mismatch between the defined end of the test and the actual end of charring. The end of the test was still set to the time when the furnace was turned off due to the following reasons: (I) it would not be possible to determine precisely when charring stopped as there might have been residual heat and smouldering in the insulation, causing charring until the specimen was cooled down with water and (II) after the burners were turned off, the specimen was no longer exposed to the standard time–temperature curve.

The uncertainty of determining the charring depth (2b) was due to some variation in the initial height of the I-joists. A minimum and maximum height was therefore defined for the I-joists, 40/41 mm for Hunton I-joists and 47/47.5 mm for Masonite I-joists. Also, for the measured residual height, for some I-joists there was a slight difference in the measured charring depth of the front and the back side of the I-joist. The difference in initial height and residual height was expressed as a minimum and maximum charring rate for the post-protected phase.

The reason why only two data points were used to find the charring rate after fall-off is explained below:

1. For Tests 1, 2 and 3, the charring front had reached the deepest embedded TC, at 18 mm depth, at the time of fall-off. In other words, there were no more measurements to include for the calculation of the charring rate.
2. For Tests 4 and 5, the fall-off happened before charring reached 18 mm, but the TC readings were after fall-off affected by the direct flame impingement on the wire and could not be used. In Test 5, the charring rate was found by combining the charring depth for the two similar-sized flanges in the same test. The I-joists were positioned in different spaces in the specimen, where the only difference between them was the centre distance between the flanges. Since they

were exposed to direct flames at different times, i.e., different fall-off times of the gypsum board, they were aligned in a graph where the time axis starts at fall-off.

2.2.3. Lateral Charring Lateral charring could not be determined in the same way as charring from the exposed side, as the start of charring along the side happened at different times corresponding to the recession of the insulation on the side. Hence, results on lateral charring in this paper were therefore based on visual inspection of the remaining cross-section area.

2.3. Method to Compare Charring Rates—Experimental Versus Design Methods

Charring rates from the experiments were compared to charring rates determined using the methods given for rectangular cross-sections in Annex C in EN 1995-1-2 [1] and for I-joists in Annex I of prEN 1995-1-2 [26].

According to EN 1995-1-2, the notional charring rate during the protected phase can be determined by Equation 1:

$$\beta_n = k_n \cdot k_s \cdot k_2 \cdot \beta_0 \quad (1)$$

where k_2 is the insulation factor of the gypsum board thickness in mm (h_p) and is given by Equation 2:

$$k_2 = 1.05 - 0.0073 \cdot h_p \quad (2)$$

For a gypsum board thickness of 15.4 mm used in these experiments, k_2 becomes 0.938. β_0 is the one-dimensional charring rate of 0.65 mm/min [1]. k_n converts the actual charring depth ($d_{\text{char},1}$) to a notional charring depth ($d_{\text{char},1,n}$) and converts the residual cross-section to a rectangular shape, as seen in Figure 8. k_s is the

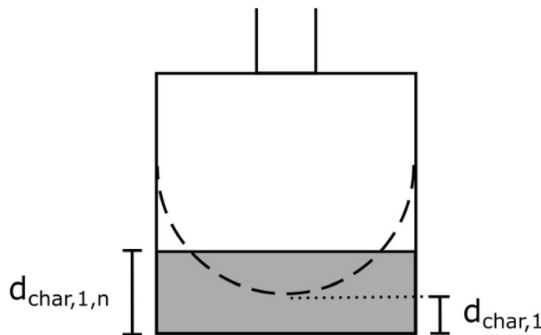


Figure 8. The remaining measured height in the experiment corresponds to the natural charring depth $d_{\text{char},1}$, while the charring depth of the design models corresponds to $d_{\text{char},1,n}$.

cross-section factor to account for different widths of the timber frame member, see Table 4.

The obtained charring rates from the experiments measured the actual charring depth, while the design methods use the notional charring depth. To compare the experimental charring rates with the design methods, the conversion factor for the corner roundings (k_n) is not taken into account (i.e., = 1).

This modified version of the charring rate will be called β_m , as given in Equation 3:

$$\beta_m = k_2 \cdot k_s \cdot \beta_0 \tag{3}$$

In prEN 1995-1-2, the notional charring rate for I-joists in the protected phase can be determined by Equation 4:

$$\beta_n = k_2 \cdot k_{s,n,1} \cdot \beta_0 \tag{4}$$

The factor k_2 is still the insulation factor for the gypsum board, but here calculated by Equation 5:

$$k_2 = 1 - \frac{h_p}{55} \tag{5}$$

For a gypsum board thickness of 15.4 mm, k_2 becomes 0.72. The one-dimensional charring rate $\beta_0 = 0.65$ mm/min [26]. The $k_{s,n,1}$ parameter is a combined conversion (k_n) and section factor (k_s) for the insulation types used in these experiments and gives the notional charring depth (Figure 8). Because we need the actual charring depth, $k_{s,n,1}$ is in this study replaced by k_s , which changes Equation 4 to be similar to Equation 3, but with different parameter values. The k_s parameter was

Table 4
Parameters for Calculation of Charring Rates for the Protected Phase, from EN 1995-1-2:2004 (Current Eurocode 5) [1] and prEN 1995-1-2:2021 (Final Draft of New Eurocode 5) [26]

Method	β_0 [mm/min]	k_n [-]	k_2 [-]	Flange width [mm]	k_s [-]	β_m [mm/min]
EN 1995-1-2	0.65	1	0.938	45	1.3	0.79
				47	1.3	0.67
				≥ 60	1.1	0.67
prEN 1995-1-2			0.72	45	1.49	0.70
				60	1.35	0.63
				90	1.18	0.55
				47	1.47	0.69
				70	1.28	0.60
				97	1.15	0.54

extracted based on the work of Mäger and Just [25] when defining the $k_{s,n,1}$ parameter and is given by Equation 6:

$$k_s = 5.43 \cdot w_f^{-0.34} \quad (6)$$

where w_f is the flange width in mm.

A comparison will reveal how both the existing model in EN 1995-1-2 [1] and the new model in prEN 1995-1-2 [26] could predict the experimental results. Such comparisons are important as they contribute to validate and improve the models.

All parameter values used in the comparison are given in Table 4.

2.4. Determination of Insulation Recession Rate

The insulation recession rate in this study was defined as the rate at which the 300°C isotherm was propagating through the insulation material, similar to the charring rate of wood and similar to other experiments studying the recession of combustible insulations [20, 28].

As the purpose of the insulation in case of fire is to protect the timber members from charring and the charring temperature of wood is approximately 300°C, the recession temperature for the insulation was also defined as 300°C.

TCs used for the determination of the recession rate were located at the interface between the gypsum board and insulation, at the centre of the insulation 100 mm into the insulation and at the upper corners of the bottom flange at depths 40.5 mm and 47 mm into the insulation for Hunton and Masonite I-joists, respectively. Figures 3 and 7 show the position of the TCs. Two different recession rates could, therefore, be calculated for each combination of I-joist type and insulation type: the recession rate at 40.5/47 mm depth and at 100 mm depth.

The recession rates were then found by Equation 7.

$$\text{recession rate [mm/min]} = \frac{\text{distance between surface TC and embedded TC}}{\text{time to reach 300°C for (embedded TC - surface TC)}} \quad (7)$$



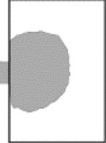
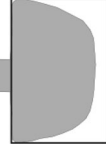
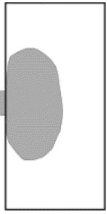
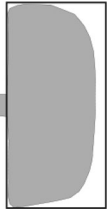

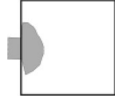
In each test specimen, there was a total of 12 corner-TCs and 8 centre insulation-TCs. The recession rates were calculated as an average of the measured rates to reduce the effect of mounting uncertainty.

3. Results





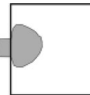


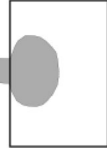
3.1. Residual Cross-Section Profiles and Measured Charring Depths

The remaining height, area and cross-section profile of the bottom flanges from all tests are presented in Tables 5 and 6. The measured charring depths for the I-joists as a function of time are presented in Figures 9, 10, 11, 12. The symbols in the figures represent the time when the TCs reached 300°C at different depths into the flanges. The time to reach fall-off of the gypsum board and the end of the tests, are marked with lines in the graphs. For some I-joists, the entire flange was



Table 5
Residual Height, Area, and Cross-Section of Flanges of Tests 1, 2 and 3

Test ID	Residual ^a			Test ID	Residual ^a		
	Height min/max [mm]	Area min/max [%] ^b	Cross-section (grey colour)		Height min/max [mm]	Area min/max [%] ^b	Cross-section (grey colour)
Test 1							
T1MaSKb	0.0	0.0		T1MaSHb	37.5/38.5	68.5/69.2	
T1MaMKb	24.5/29.0	23.8/29.0		T1MaMHb	39.0/39.5	71.6/72.4	
T1MaLKb	24.5/25.0	25.0/25.0		T1MaLHb	41.0/41.0	77.0/77.1	
Test 2							
T2HuSCif	0.0	0.0		T2MaSCif	8.5/10.5	6.8/9.2	

**Table 5
continued**

Test ID	Residual ^a				Test ID				Residual ^a				
	Height min/max [mm]	Area min/max [%] ^b	Cross-section (grey colour)		Test ID	Height min/max [mm]	Area min/max [%] ^b	Cross-section (grey colour)		Test ID	Height min/max [mm]	Area min/max [%] ^b	Cross-section (grey colour)
T2HuMCIf	0.0	0.0			T2MaMCIf	13.5/15.5	14.9/17.6						
T2HuLCIf	8.5/10.5	2.3/3.0			T2MaLCIf	20.0/21.0	30.8/32.3						
Test 3													
T3HuSHIf	15.0/16.5	13.2/13.4			T3MaSHIf	0.0	0.0						
T3HuMHIf	19.0/20.0	20.3/22.4			T3MaMHIf	22.0/23.5	19.2/18.5						

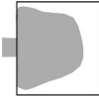
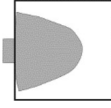
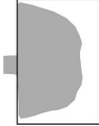



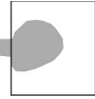
**Table 5
continued**

Test ID	Residual ^a			Test ID			Residual ^a		
	Height min/max [mm]	Area min/max [%] ^b	Cross-section (grey colour)	Test ID	Height min/max [mm]	Area min/max [%] ^b	Cross-section (grey colour)		
T3HuLHif	26.0/27.5	39.2/40.1		T3MaLHif	27.5/30.0	27.5/32.7			





^aThe minimum and maximum height are measured on both ends of the ~ 50 mm piece cut from the I-joist after the test

^bPercent of the original area

Table 6
Residual Height, Area, and Cross-Section (grey colour) of Flanges of Tests 4 and 5

Test ID	Residual ^a			Test ID	Residual ^a		
	Height min/max [mm]	Area min/max [%] ^b	Cross-section (grey colour)		Height min/max [mm]	Area min/max [%] ^b	Cross-section (grey colour)
Test 4 T4HuSHb	30.0/30.5	54.3/54.6		T4MaSHb	32.5/34.0	45.4/52.6	
T4HuMHb	30.0/30.5	56.7/58.9		T4MaMHb	33.0/34.5	50.3/53.1	
T4HuLHb	32.5/32.5	67.8/70.5		T4MaLHb	35.5/36.0	57.3/57.6	
Test 5 T5HuSHb	24.5/24.5	24.6/28.0		Not tested			

**Table 6
continued**

Test ID	Residual ^a			Test ID	Residual ^a		
	Height min/max [mm]	Area min/max [%] ^b	Cross-section (grey colour)		Height min/max [mm]	Area min/max [%] ^b	Cross-section (grey colour)
T5HuMHb	23.5/24.5	29.8/32.7		T5HuMHbcc60	21.0/21.0	26.1/26.9	
T5HuLHb	25.0/25.5	41.9/45.1		T5HuLHbcc60	22.5/23.5	35.4/38.3	

^aThe minimum and maximum height are measured on both ends of the ~ 50 mm piece cut from the I-joist after the test

^bPercent of the original area

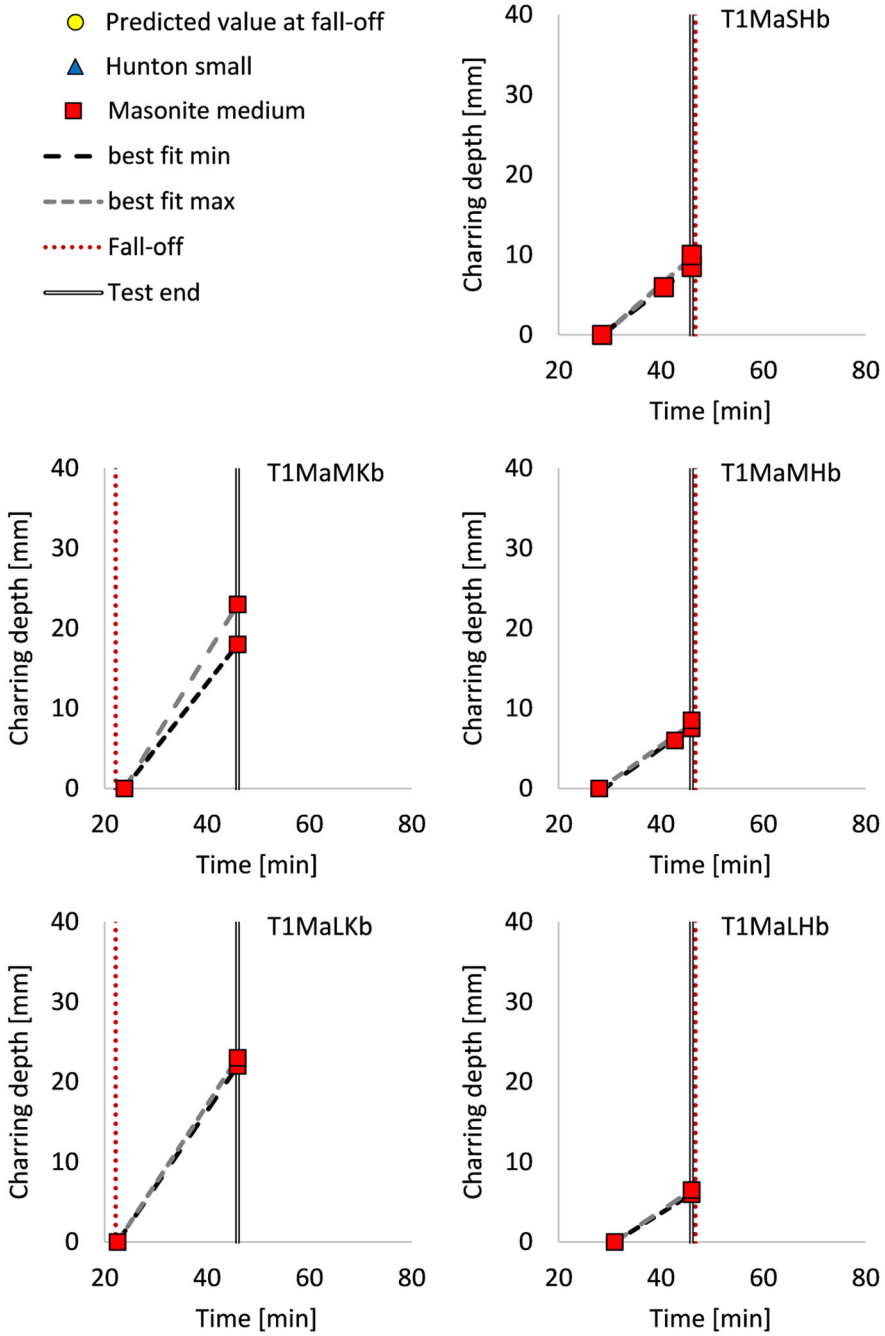


Figure 9. Test 1—Charring of flange from the exposed side.

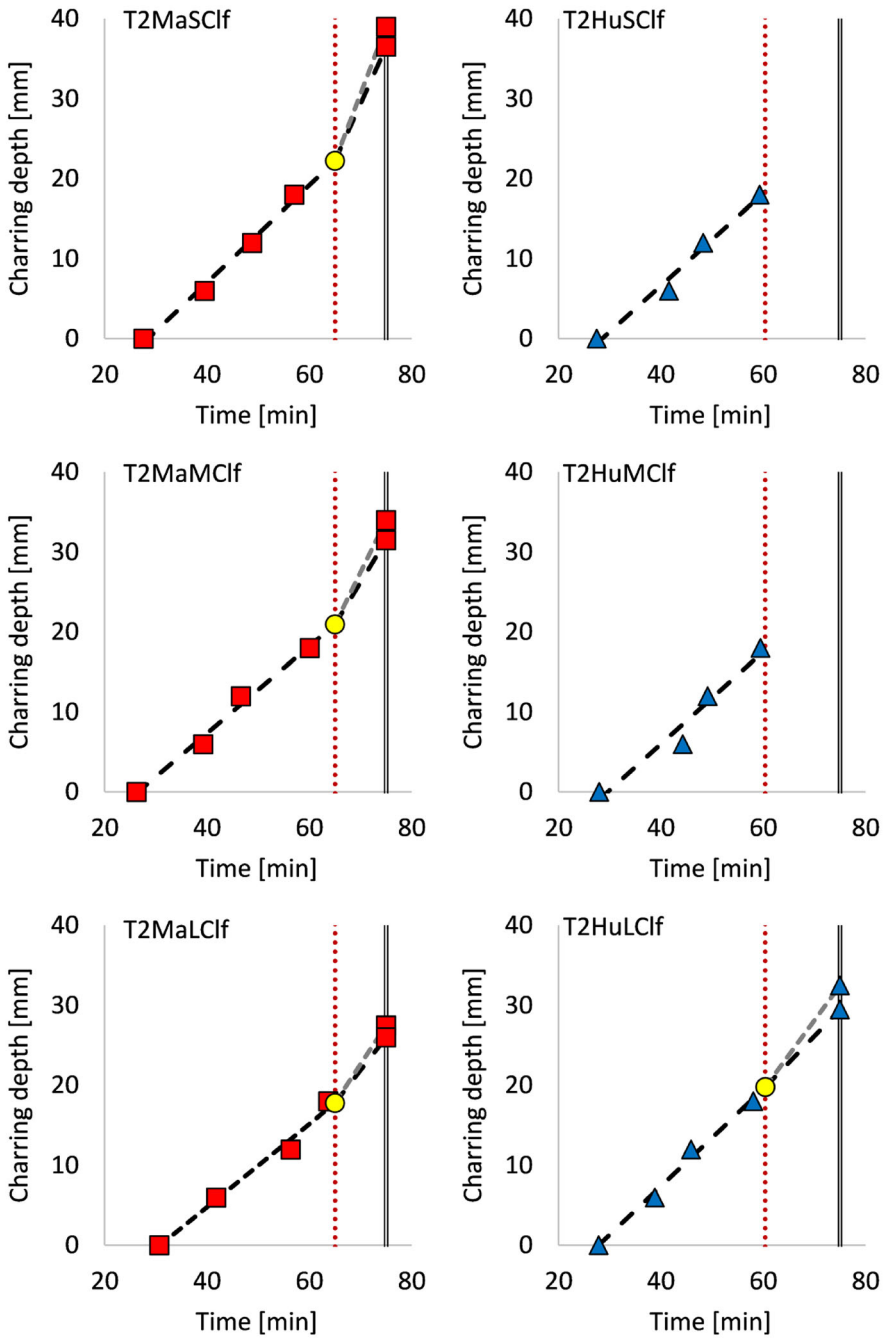


Figure 10. Test 2—Charring of flange from the exposed side.

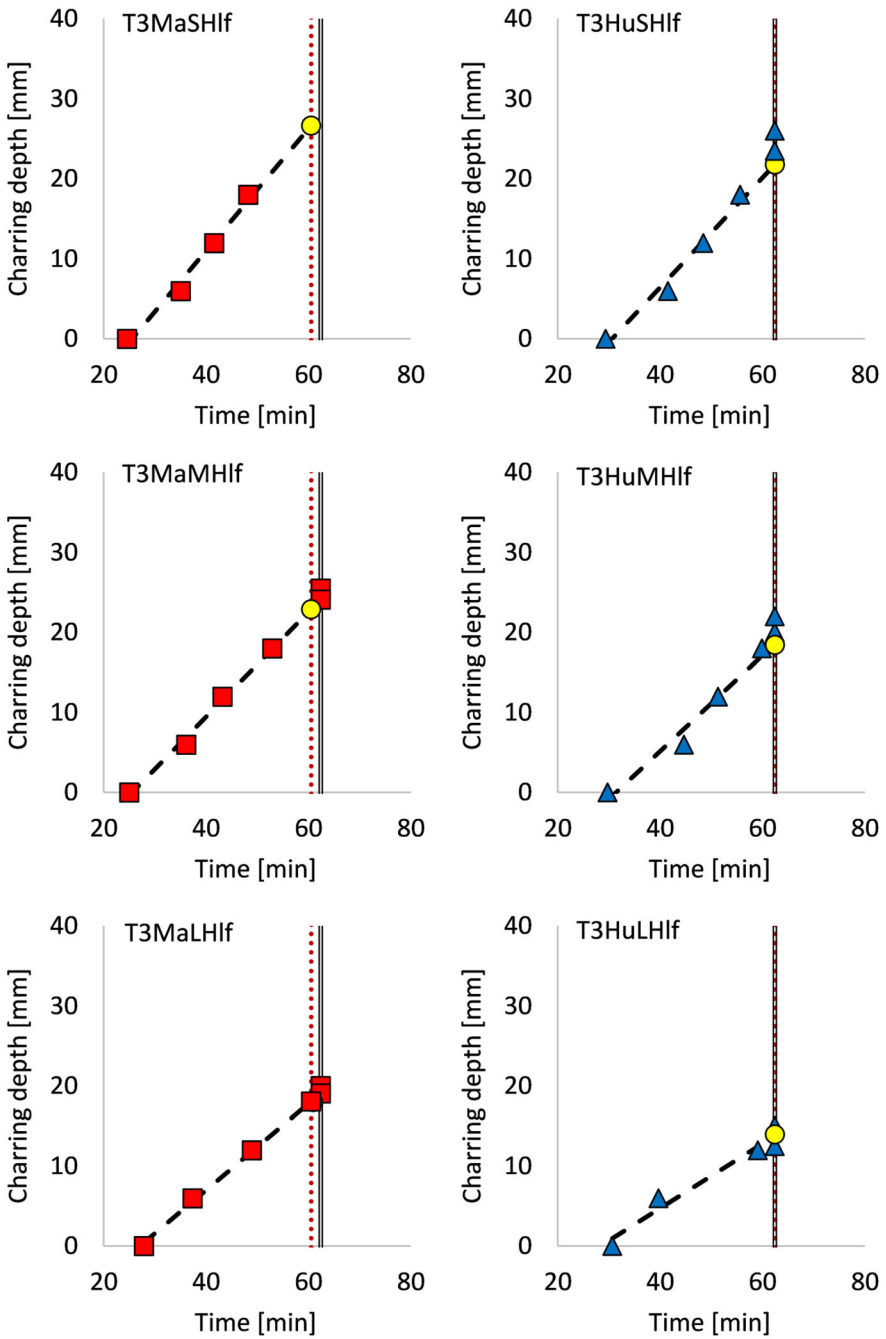


Figure 11. Test 3—Charring of flange from the exposed side.

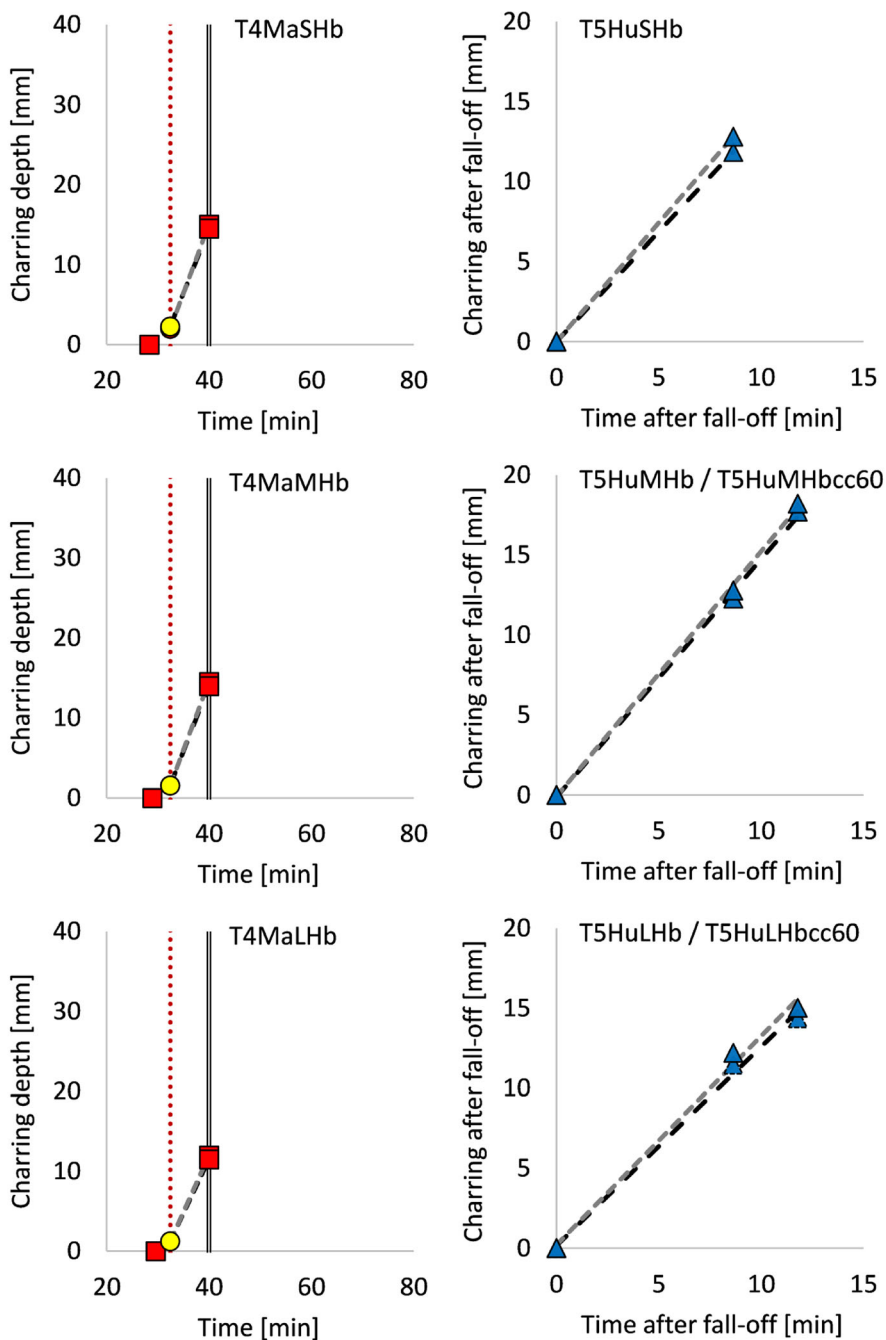


Figure 12. Test 4 (left) and Test 5 (right)—Charring of flange from the exposed side.

charred through at the end of the test. It is not known precisely at which time the flange was completely charred. The final charring depth for those flanges is, therefore, not included in the figures.

In Figure 13, the reduction of cross-section area influenced by different fall-off times of gypsum plasterboards is shown. In Figure 14, the reduction of cross-section area influenced by insulation fall-down is shown.

3.2. Charring Rates for I-joists

The calculated charring rates are given in Table 7 and are based on the procedure described in Sect. 2.2. The results with Hunton I-joists from Test 4 are not included in the table due to the short duration of the post-protection phase, which caused too large uncertainties in the calculation.

A few of the flanges were totally charred. In test T1MaSKb, the entire flange and about 25 mm of the web were charred. In test T2HuMClf, the entire flange and about 5 mm of the web were charred. For T2HuSCLf, the entire flange was charred, but the web had not been charred. The charring rates for these three tests were calculated based on charring of the full flange height and is set to larger or equal (\geq) to the calculated charring rate.

Start of charring on the flanges of the I-joists is given as t_{ch} in Table 7. a_{1max} is the calculated maximum charring rate and a_{1min} is the calculated minimum charring rate in the protected phase. While a_{2max} and a_{2min} are the calculated charring rates in the post-protected phase.

3.3. Comparison of Charring Rates Against Design Methods

A comparison between the experimental charring rates and the calculated values based on EN 1995-1-2 and prEN 1995-1-2 was made. This was performed according to the method in Sect. 2.3.

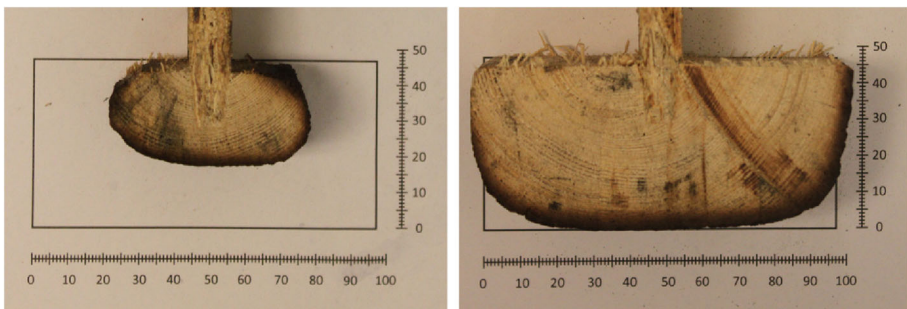


Figure 13. The protective effect given by the gypsum board is shown by comparing two flanges from Test 1, where the left flange experienced a gypsum board fall-off at 22 min, while the right flange was protected by the gypsum board throughout the test (to 45 min). The rectangular shape is the original flange size. Numbers are in mm.

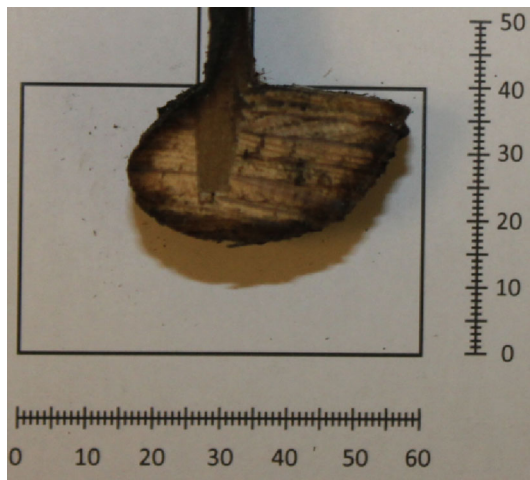


Figure 14. Example of a medium-sized Hunton flange in Test 5 with a highly irregular shape. The flange experienced insulation fall-down during the test on one side, resulting in the irregular shape. The rectangular shape is the original flange size. Numbers are in mm.

The values of all design parameters and the corresponding charring rates are summarised in Table 4, while the comparison is given in Table 8. Due to the short protected phase of Test 1 with phenolic insulation and Test 4 and 5 with wood fibre batts, it was not possible to calculate a charring rate in the protected phase for those tests. Hence, the table does not include values for those tests.

3.4. Recession Rates for Combustible Insulation

The average time for the 300°C isotherm to reach the TCs in the insulation and on the interface between the insulation and I-joist flange was measured in the tests. Recession rates for the different insulations have been calculated based on the procedure in Sect. 2.4 and are given in Table 9.

In all tests, the TCs at the corners reached 300°C and the recession rate of the insulation next to the flange could therefore be determined. However, in only one test, the centre TCs at 100 mm depth into the insulation reached 300°C. The recession rate for the other tests not reaching 300°C was therefore set to “less than” (<).

The results show that the recession rate was lower, close to the flange, than between two I-joists.

In most tests, the recession rate was obtained for exposure mainly in the protected phase. However, recession of the phenolic batt was only measured in the post-protected phase because the gypsum board fell down early.

The wood fibre batts were used in several tests and the average recession rate at the corner for all tests was 3.3 ± 0.7 mm/min, based on 26 values.

Table 7
Calculated Charring Rates on the Fire Exposed Side of the I-Joists from the Experiments

Test ID	t_{ch} [min]	Gypsum board fall-off [min]	End of test [min]	Protected phase		Post-pro- tected phase	
				Charring rate		Charring rate	
				a_{1min} [mm/min]	a_{1max} [mm/min]	a_{2min} [mm/min]	a_{2max} [mm/min]
Test 1							
T1MaSKb	23.7	22.2	45	–	–	$\geq 2.13^a$	
T1MaMKb	23.9			–	–	0.81	1.04
T1MaLKb	22.5			–	–	0.94	0.98
T1MaSHb	28.5	46.5		0.49	0.56	–	–
T1MaMHb	28.0			0.45	0.45	–	–
T1MaLHb	31.0			0.40	0.43	–	–
Test 2							
T2HuSClf	27.5	60.4	75	0.58		$\geq 1.55^a$	
T2HuMClf	28.0			0.58		$\geq 1.59^a$	
T2HuLClf	27.9			0.61		0.67	0.87
T2MaSClf	27.6	65.0		0.61		1.43	1.68
T2MaMClf	26.2			0.54		1.05	1.30
T2MaLClf	30.7			0.52		0.82	0.97
Test 3							
T3HuSHlf	29.4	62.4	62.5	0.69		–	–
T3HuMHlf	29.8			0.60		–	–
T3HuLHlf	30.7			0.40		–	–
T3MaSHlf	24.6	60.5		0.76		–	–
T3MaMHlf	25.0			0.65		0.65	1.39
T3MaLHlf	27.8			0.54		0.54	1.03
Test 4							
T4HuSHb	30.2	38.3	40	–		–	–
T4HuMHb	30.2			–		–	–
T4HuLHb	31.5			–		–	–
T4MaSHb	28.4	32.4		–		1.61	1.72
T4MaMHb	28.9			–		1.64	1.71
T4MaLHb	29.6			–		1.36	1.44
Test 5							
T5HuSHb	30.0	36.5	45	–		1.37	1.49
T5HuMHb + T5HuMHbcc60	27.1	36.5		–		1.49	1.53
	30.5	33.3					
T5HuLHb + T5HuLHbcc60	29.5	36.5		–		1.24	1.31
	28.4	33.3					

^aThe flange was completely charred at the test end

^bNo R^2 value is given when only two data points are present

Table 8
Charring Rates Calculated Based on Results from the Experiments
During the Protected Phase Compared to Calculated Charring Rates
Based on EN 1995-1-2:2004 (Current Eurocode 5) [1] and prEN
1995-1-2:2021 (Final Draft of the New Eurocode 5) [26]

Test ID	Experimental	EN 1995-1-2:2004		prEN 1995-1-2:2021	
	$a_{1\max}$ [mm/ min]	β_m [mm/ min]	$\beta_m - a_{1\max}$ [mm/ min]	β_m [mm/ min]	$\beta_m - a_{1\max}$ [mm/ min]
Test 1					
T1MaSHb	0.56	0.79	0.23	0.69	0.13
T1MaMHb	0.45	0.67	0.22	0.60	0.15
T1MaLHb	0.43	0.67	0.24	0.54	0.10
Test 2					
T2HuSClf	0.58	0.79	0.22	0.70	0.12
T2HuMClf	0.58	0.67	0.09	0.63	0.05
T2HuLClf	0.61	0.67	0.06	0.55	− 0.06
T2MaSClf	0.61	0.79	0.18	0.69	0.08
T2MaMClf	0.54	0.67	0.13	0.60	0.05
T2MaLClf	0.52	0.67	0.15	0.54	0.02
Test 3					
T3HuSHlf	0.69	0.79	0.11	0.70	0.01
T3HuMHlf	0.60	0.67	0.07	0.63	0.03
T3HuLHlf	0.40	0.67	0.27	0.55	0.15
T3MaSHlf	0.76	0.79	0.03	0.69	− 0.08
T3MaMHlf	0.65	0.67	0.02	0.60	− 0.06
T3MaLHlf	0.54	0.67	0.13	0.54	0.00

4. Discussion

4.1. Charring of I-Joists

4.1.1. Charring Rates on Fire Exposed Side 4.1.1.1. Protected Phase For the protected phase, a best-fit analysis was used, including several data points ranging over a relatively long time span (up to 38 min) (Table 7). The calculated charring rates of the protected phase are therefore considered to be quite accurate. This is supported by the good linear match of the data points.

Although the Masonite (solid) and Hunton (LVL) I-joists were manufactured with different components, their charring rates were in the same range in comparable tests. The charring rates varied from 0.40–0.76 mm/min to 0.40–0.69 mm/min for Masonite and Hunton I-joists, respectively. In most of the comparable tests, the Hunton I-joists had a slightly lower charring rate than the Masonite I-joists, see Table 7. In general, the charring rate decreased with increasing flange width, which is as expected [1]. The reason being that for wider flanges, less heat from the lateral sides reaches the centre of the flange, where the TCs to monitor charring are located. And the effect of the corner rounding is smaller for wider flanges.

Table 9
Recession Rates for the Different Insulation Products

Test no	Insulation	Recession rate \pm std. deviation [mm/min]	Average time to reach 300°C after start charring		Based on (at depth)
			Protected [min]	Post-protected [min]	
1	Wood fibre batt	2.7 ± 0.3	18	0	6 corner TCs (47 mm)
		$< 4.9^a$	21	0	4 insulation centre TCs (100 mm)
1	Phenolic foam batt	5.7 ± 2.3	0	9	6 corner TCs (47 mm)
		6.8 ± 1.2	0	15	4 insulation centre TCs (100 mm)
2	Cellulose loose-fill	1.1 ± 0.04	39	3	12 corner TCs (40.5/47 mm)
		$\leq 2.2^b$	39	12	8 insulation centre TCs (100 mm)
3	Wood fibre loose-fill	2.3 ± 0.5	20	0	12 corner TCs (40.5/47 mm)
		4.1 ± 0.7	25	0	8 insulation centre TCs (100 mm)
4	Wood fibre batt	3.6 ± 0.9	11	2	12 corner TCs (40.5/47 mm)
		$< 7.0^a$	11	5	8 insulation centre TCs (100 mm)
5	Wood fibre batt	3.1 ± 0.4	12	1	10 corner TCs (40.5 mm)
		$< 7.9^a$	12	5	7 insulation centre TCs (100 mm)

^aNone of the centre TCs had reached 300°C when the test was ended. The actual recession rate is likely to be slower than the value in the table

^bOnly 2 of 8 centre TCs reached 300°C. 2.2 mm/min was the maximum of those two values

4.1.1.2. Post-protected Phase The charring rates in the post-protected phase ranged from 0.54 mm/min to 1.72 mm/min when excluding the I-joists where the flange was fully charred. This was higher than charring rates in the protected phase, as expected. The charring rates were obtained from only two data points with some related uncertainties (see Sect. 2.2.2). In addition, this phase had a shorter duration. These effects combined imply that there was a higher degree of uncertainty related to the charring rates in the post-protected phase and no comparison is made with the design models.

Although the charring rates have some uncertainties, the maximum charring rate for this phase is believed to be on the conservative side due to the following reasons:

- Measurement uncertainties, e.g., measured remaining height of the flange, were included in the calculation.
- The end of the test was defined as when the furnace burners were shut off since the fire exposure would no longer be according to the standard time–temperature curve. However, the pyrolysis process of the I-joists continued for a short period (~ 2 min) between the burner shut-off and extinguishment.

The measured charring depth is, therefore, probably a bit larger than it was at the end of the test. The consequence is that the calculated charring rates after fall-off are somewhat higher than the actual rate in the fire test. For the tests where the post-protection phase was short, this effect becomes more prominent.

The design model for I-joists developed by Mäger and Just [24, 25] consists of four phases, where Phases 3 and 4 occur after gypsum board fall-off and Phase 4 is recognised by a reduced slope as the charring layer reaches 25 mm, see Figure 2. In this case, observing such a slope reduction has not been possible for several reasons. To observe the change from Phase 3 to Phase 4, the post-protected phase must be sufficiently long for a 25 mm char layer to be formed and a sufficient number of TCs to measure the charring depth must be present. In this test series, the TCs were either malfunctioned (Test 4 and Test 5) after fall-off, or the deepest embedded TC had already reached 300°C at the time of fall-off. These two effects caused the charring rate of the post-protected phase to be based on the measurements at two charring points only, i.e., the charring depth at fall-off and the final charring depth at the test end. This is described in detail in Sect. 2.2.2. In addition, several flanges were charred less than 25 mm during the whole test.

A learning outcome of these experiments is to use sheathed TCs for future tests, as they can better withstand direct flame exposure to the wire without affecting the TC readings at the junction. Related to this test series, such a change would have provided more data points for the analysis of Test 4 and Test 5, thereby reducing the uncertainty of the charring rate for the post-protected phase. Sheathed TCs would also have allowed for smaller drilled holes which had reduced any convective heat transfer through the holes.

4.1.2. Lateral Charring and Remaining Cross-section Area As seen in Tables 5 and 6, the remaining cross-section of the flanges had the characteristic trapezoid-like shape for short exposures (Test 1 and 4) and a more rounded shape for longer exposures (Test 2 and Test 3). These characteristic shapes were due to the lateral charring, which became more dominant when the insulation degraded as the lateral sides were more and more exposed.

In Test 1 with wood fibre batt insulation and Test 3 with wood fibre LF insulation, several flanges were heavily charred on the lateral side, although there was barely any post-protected phase. This highlights that lateral charring of the flanges of an I-joist should not be neglected in the protected phase. I-joists are vulnerable to charring due to the thin cross-section, while rectangular beams are more resilient. Therefore, even limited charring of the lateral sides of the flanges must be considered. This is a difference compared to charring of rectangular beams, where lateral charring, in general, is not considered in the protected phase [20].

In Test 1, due to the early fall-off of the gypsum board (Table 7), the flanges protected by the phenolic insulation experienced only a post-protected phase. The gypsum board on the other half remained until the end of the test and the flanges protected with wood fibre batt insulation were only exposed in the protected phase. The difference between them was clearly visible (Figure 13). The flanges only experiencing the protected phase were barely charred on the lateral side and charred only 6–9 mm on the fire-exposed side. The flanges only experiencing the post-protected phase were heavily charred from the lateral sides, had more rounded corners and charred approx. 22 mm on the fire-exposed side on the two largest flange sizes.

It is obvious that this difference was related to the tougher thermal exposure for the I-joists and insulation on the phenolic foam side when not protected by the gypsum board. Based on video analysis and TC readings, the insulation was present in both Spaces A and B at the end of the test. This can rule out that insulation fall-down contributed to the difference seen.

Since two different insulation types were used, the recession speed of the two would also contribute to the different char depths. Based on the available data, the recession speed for the wood fibre batt was 2.7 mm/min (protected phase) and 5.7 mm/min (post-protected) for the phenolic foam batt. The latter corresponds to 4.1 mm/min with a conversion to the protected phase (see Sect. 4.2.1), which is about 50% higher than the wood fibre insulation. A different charring would therefore have been expected also with similar heating exposure.

In this test, it is unclear what triggered the early fall-off on one side of the test specimen. However, early fall-off has been related to both the insulation type and the screw distance from the edge of the board [37].

In this test, there was no temperature difference on the back side of the two gypsum boards until 18 min. After this point, the temperature on the side with phenolic foam insulation increased faster than on the other side, probably due to the higher R-value (Table 2). Gypsum board fall-off happened at around 340°C, which was considerably lower than the backside temperature of the other gypsum boards in the other tests. It, therefore, seems unlikely that the gypsum board fell off due to heat alone, but probably with contribution from a crack.

Test 2 had the longest exposure, with a total test time of 75 min. The small and medium flanges of the Hunton I-joists were fully charred, while a small fraction of the large flange was remaining. Compared to the Masonite I-joists of the same test, none of the flanges was fully charred, although these also were heavily charred. The difference in charring between the Hunton and Masonite I-joists can be explained by two reasons: (a) The Hunton I-joists had a 5 min longer post-protected phase. (b) The Hunton flange height was initially 7 mm shorter and the small and medium Hunton flange widths were 2 mm and 10 mm smaller than the Masonite small and medium flange, respectively.

The shorter flange height influences the maximum time a flange can be exposed before it is fully charred from the exposed side. It also influences the time until the lateral side of the flange becomes fully exposed due to insulation recession. As the recession rate of the insulation was about 1.1 mm/min in this test, this means

that the lateral side of the Hunton I-joists became fully exposed about 7 min before the lateral side of the Masonite I-joists.

The reduced flange width influenced the charring in several ways: Firstly, by the time until the flange was fully charred due to lateral charring. Secondly, the smaller width contributed to a faster charring from the exposed side [1]. Thirdly, it affected the time until the flange was charred from three sides, as explained above.

As Test 2 had both a protected and post-protected phase, it was not straightforward to assess how much of the lateral charring that happened in each of the two phases.

When comparing the remaining cross-section area of Masonite I-joists of Test 2 and Test 3, it was seen that the corners of the exposed flanges (marked as “TC corner” in Figure 3) were less rounded in Test 2, although this test had a longer exposure. The reason for this was the particularly low recession rate, 1.1 mm/min, of the cellulose LF insulation in Test 2. In comparison, the recession rate of the wood fibre LF insulation in Test 3 was 2.3 mm/min. In Test 2, the lateral sides of the Masonite flanges were fully exposed due to insulation recession at 69 min on average, while in Test 3, the lateral sides were fully exposed at 43 min on average.

For T3MaSHlf, there was a good linear fit for the data points in the protected phase, see Figure 11. However, the predicted charring depth at fall-off does not correspond with the fact that the flange was fully charred, see Figure 11 and Table 5. Based on the linear prediction, the charring depth of the flange at fall-off should have been about 27 mm, with 20 mm left to be charred. As the post-protected phase only lasted for about two minutes, to get the flange fully charred, the charring rate must have been about 10 mm/min. This is many times higher than typical charring rates in the post-protected phase and is not realistic. Another effect must have been present.

The most likely explanation is related to the effect of the lateral charring. Compared with a similar test, T3HuSHlf, with the same insulation and approximately the same flange size, see Table 5, it is clear that the lateral charring has played a significant role in the protected phase of this test. There were just a few millimetres left on the lateral sides of the flange before the integrated web was reached. As the start of charring occurred earlier for T3MaSHlf and it was exposed to direct flames longer than T3HuSHlf, it is likely that the flange was totally charred due to lateral charring.

In Test 3, the lateral sides of the flange were totally exposed at about 43 min, i.e., no insulation remained covering the originally 47 mm wide flange. To reach complete charring of the flange in this test, the average lateral charring rate must have been larger than 1.2 mm/min, which seems likely.

At the beginning of the charring process, the charring on the exposed and lateral sides can almost be treated as two independent processes. However, as the charring proceeded, the solid volume of the flange decreased. The ability to transport heat away from the charring zone and further into the wood was thereby reduced. This resulted in an increased heat accumulation in the remaining flange with a corresponding increased heat propagation rate through the material. It is likely that the flange at one point reached a critical remaining volume where the charring on the exposed and the lateral side could no longer be treated as inde-

pendent processes. Instead, they must be treated as interdependent processes. The charring rate in this phase was naturally higher than at the beginning of the charring process. The smaller the original flange was, the more prone the flange was to get affected by this effect. The large difference in charring rate between the small and medium-sized flange in test 1 with phenolic batt insulation was likely caused by this effect. This effect should be studied more and possibly added to the design method.

For Test 4, the Masonite I-joists had a smaller remaining cross-section area than the Hunton I-joists. This was likely caused by the duration of the post-protected phase, which was 6 min longer for the Masonite I-joists.

In Test 5, several flanges had a non-symmetrical remaining area, particularly the top corners of the flange (Figure 14). This can be explained by the fact that three of seven insulation batts fell down during the test. However, none of the flanges lost both adjacent insulation batts. The fall-down happened after the lateral side had been fully exposed, so the fall-down did not affect the calculated recession rate of the insulation. However, the fall-down caused the inner side flange, where the web was attached, to be exposed. This caused an increased charring of the upper corner area, as seen in Table 6 and Figure 14.

In several tests, there were large differences in remaining cross-sections between the flange sizes (Table 5). The corner rounding due to charring had a larger effect on the narrow flanges than the wider ones. The height of the residual cross-section was, therefore, smaller. In addition, the wider flanges provided longer protection of the web because it took more time to char through from the lateral sides.

In general, insulation that is adapted to the I-joist profiles protects the web and flange on two sides (lateral and inner side of the flange). Without this insulation, the flange is exposed from three sides (exposed, lateral and inner) and the web becomes directly exposed to fire. Charring from these sides and the web will quickly reduce the load-bearing capacity [38].

As explained in Sect. 2.2, it was not possible to retrieve TC readings throughout the whole test duration from all tests. This resulted in different quality of charring and recession data for the different combinations of I-joists and insulation types. Further work is, therefore, needed to fill the gaps in this study and should also include other insulation types.

4.1.3. Comparison with Calculation Methods The experimental results for the charring rate in the protected phase, see Table 8, were lower than the predicted charring rate of EN 1995-1-2 [1] for rectangular cross-sections. The difference was on average 0.14 ± 0.08 mm/min lower.

The experimental charring rates were also compared with rates calculated based on the proposed new design method for I-joists in prEN 1995-1-2 [26], see Table 8. The experimental charring rate was on average 0.05 ± 0.08 mm/min lower than calculated. The minimum value was 0.15 mm/min lower than the calculated and the maximum value 0.08 mm/min higher. Related to this data set, the charring rates predicted by the new design method in prEN 1995-1-2 were more accurate than the predicted charring rate of the current design method in EN 1995-1-2.

4.2. Recession of Combustible Insulation

4.2.1. Recession Rates Both the wood fibre and cellulose loose-fill insulations degraded slowly, with an average recession rate measured at the corners of the flanges of about 1.1 mm/min (protected phase) and 2.3 mm/min (protected phase), respectively. The wood fibre batt and the phenolic foam had a slightly higher recession rate, with 3.3 mm/min (protected phase) for the wood fibre batt and 5.7 mm/min (post-protected phase) for the phenolic foam batt. See Table 9.

Due to an early fall-off of the gypsum board (Table 7), the phenolic insulation had its whole exposure in the post-protected phase. To compare the recession rate with the other insulation products, which mainly were exposed in the protected phase, one can multiply it with the insulation factor k_2 for the protected phase (see Sect. 2.3). This gives a recession rate of 4.1 mm/min, which is closer to the other values but still higher.

An overview of recession rates for wood fibre, cellulose, glass wool and stone wool is presented in Table 10. Most of them were obtained in the post-protected phase. Therefore, to compare the results to the other values, the recession rate must be divided by a factor of 0.72, the k_2 value for type F gypsum board used in the tests, see Equation 5. Still, with this correction, all the insulation types had a recession rate lower than typical values found for glass wool (5–28 mm/min) [14, 39].

The values of both loose-fill insulations in this test series had about the same recession rate as the value given for stone wool [39]. However, further testing is needed to confirm this.

Regarding wood fibre and cellulose insulation, the recession rates obtained in this test series are in line with the lowest obtained values previously reported [23, 28] (Table 10).

Another reason for the large difference in recession rates might be different shrinking properties of the insulations and the use of rectangular cross-sections and not I-joists, as discussed in Sect. 4.2.2.

Table 10
Overview of Recession Rates for Different Insulation Types

Research	Insulation type	Recession rate	Phase
Winter et al. [28]	Cellulose, loose-fill	1–2 mm/min	Protected
Winter et al. [28]	Cellulose, loose-fill	2–5 mm/min	Post-protected
Tiso and Just [23]	Cellulose, batt	13.4 mm/min	Post-protected
Winter et al. [28]	Wood fibre, batt	2–4 mm/min	Protected
Winter et al. [28]	Wood fibre, batt	4–16 mm/min	Post-protected
Manguse [39]	Stone wool, batt	2.7 mm/min	Mix of protected and post-protected
Just [14]	Glass wool, batt	15–28 mm/min	Post-protected
Manguse [39]	Glass wool, batt	4.6–11.1 mm/min	Post-protected

Further testing is needed to confirm the large variation of recession rates seen for glass wool and the values of both loose-fill insulations, which were lower than observed values for stone wool (Table 10).

In most of the tests performed in our study, the TCs at 100 mm depth in the middle of the insulation did not reach 300°C during the test and the recession rates in those tests could only be set to a “less than” value, based on the test duration. These rates could, therefore, not be compared with the recession rates determined based on the measurements from the TCs on the corner of the flanges.

For the few tests where the TCs in the insulation reached 300°C, the recession rates were higher than those of the same tests measured close to the flanges, see Table 9. This is probably due to the thermal properties of the I-joist compared to the insulation. The heat conduction coefficient of wood is many times higher than for the insulation materials. Hence, in the interface between insulation and I-joist, heat will be transported from the insulation to the flange as a heat sink. This reduces the heating of the insulation close to the flange compared to the bulk part of the insulation.

4.2.2. The Effect of Shrinking on the Recession Rate As discussed in Sect. 4.2.1, the recession rates in this test series were substantially lower than several of the previously reported values for similar insulation types. There are several reasons which could explain this difference. One reason is related to the reported values being measured in the post-protected phase, as discussed in Sect. 4.2.1. This effect, however, does not compensate for the whole difference. Regarding the recession rates of prEN 1995-1-2 [26], these are generic values, meaning that they are the highest measured in a sample, to be on the conservative side.

Another effect may be related to shrinking of the insulation. In general, the shrinking affects the ability of the insulation to protect the wood member in two ways: (a) shrinkage reduces the insulation height and thereby the lateral side of the wood member becomes more exposed, (b) when the insulation shrinks, a small gap between the wood member and the insulation occurs. This small gap allows for a convective heat transfer through this gap. The TCs on the lateral side of the wood member used to evaluate the recession rate are then heated up in correlation with the size of the gap and, thereby, the shrinking properties of the insulation.

Most reported recession rates were obtained in a different test setup, with rectangular members and not I-joists. The recession rate was measured at 100 mm depth, not 40.5 mm/47 mm, as in this test series.

As the insulation degraded past the flanges in all tests before the test was terminated, it was not possible to assess whether a gap had been formed between the flange and the insulation. However, for most of the tests with wood fibre batts, the insulation remained in the cavity after extinguishing and there was no visible gap between the insulation and the web, indicating negligible shrinking. In the tests with wood fibre batt, the batt had been cut larger than the cavity and compressed into the cavity. This compression affected the test result in two ways, the insulation was less prone to fall down and the oversizing compensated for any

shrinking. This is an advantage which may be utilised for compressible insulation types.

For the phenolic batt, the insulation was still in the cavity after the end of the test, although a small gap was observed a few places. However, as the insulation had been cut to match the flange-to-flange distance, this caused a gap between the insulation and the web, which was filled with small pieces of phenolic batt. The small observed gaps may then have been due to displacement of the small insulation pieces. However, the fact that the batts stayed in place after the test indicates little or negligible shrinking.

For the test where the insulation fell down during the extinguishing process (Test 2—cellulose LF), it was possible to locate precisely where the insulation had been due to a distinct division between charred and uncharred wood on the web. This division proves that shrinking had a negligible effect in this test series.

For the wood fibre LF insulation—Test 3, it was not possible to assess the shrinking property as the insulation fell down before the test ended. The recession rate, however, was not affected by this as the insulation had degraded past the flange at the time it fell down.

Another observation which influenced the recession rates was the time until the corner flanges had reached 300°C. This time could vary up to several minutes in the same test with the same flange height and the same insulation and is shown through the standard deviation in Table 9. No trend was seen related to the size of the flange. Instead, this was believed to be directly related to how tight the insulation was fitted to the flange. This explanation also matches the ability of the insulations to be compressed and oversized. The loose-fill insulations and the compressible wood fibre batt had all quite uniform recession rates, i.e., a low standard deviation. The phenolic foam, however, had a large standard deviation and was the only incompressible insulation.

4.2.3. Insulation Fall-Down In general, insulations not fastened to the timber frame are vulnerable to fall-down when the cladding falls off. The loadbearing capacity of floors made of I-joists is particularly vulnerable to insulation fall-down, as floors made of I-joists are likely to fail when the web is burned through, even if the bottom flanges are partly remaining [38].

Regarding the loose-fill insulations, wood fibre LF fell down almost immediately after fall-off of the gypsum board, while the cellulose LF stayed in place until the end of the test, more than 10 min after fall-off of the gypsum board. The different behaviour may have been caused by how the insulations were filled into the cavities, where the cellulose LF was blown-in and the wood fibre LF was manually packed. It is believed that blown-in insulation sticks better together and acts more like a batt than the loose-fill insulation that was manually packed. For future tests, the blown-in method would be recommended for loose-fill insulation types, as it is more realistic and seems to stay better in place.

In Test 4, the wood fibre batts did not fall down during the test. This is believed to be because the batts were cut larger than the cavity opening. The cut profile to match the flange probably also helped keeping them in place. However, in Test 5, three of seven batts fell out during the test. The most probable reason is

that the batts by accident were cut with a less oversize than in the other tests. The fall-down in Test 5 made it hard to compare the effect of the insulation width, 400 mm versus 600 mm. However, the fall-down gave a reminder of the importance of holding the insulation in place, see Figure 14. The flange side with no insulation had a more rounded shape and the remaining cross-section was effectively reduced compared to the flange side with insulation still in place. In addition, the lack of insulation also makes the web exposed to the fire and the I-joist more vulnerable to failure [38].

Most of the insulation products did not fall down during the test and this is likely due to how they were installed, like cut to match the I-joists profile and oversizing the insulation batts. However, such an installation procedure is time-consuming, hard to repeat precisely and most likely will not be followed each time in an actual building. Therefore, precise instruction details and adapted tools for cutting the flange profiles are needed if this oversizing should be implemented in actual installations.

However, the blown-in loose-fill insulation is different. Firstly, it fills the whole cavity without any need for tailor-made insulation batts and is less time-consuming. Secondly, the process is highly repeatable and since the blown-in method must be performed by a certified worker, this ensures that testing in a lab is realistic to how it will be in an actual building.

In this test series, cellulose LF had the lowest recession rate and showed a good ability to stay in place after gypsum board fall-down. This shows that it is possible to protect the I-joists well without time-consuming and less repeatable tailor-made solutions.

4.2.4. Classification of Insulation Products In prEN 1995-1-2 [26], insulations are given a classification, a so-called protection level (PL), due to how they degrade in a furnace test. That setup is similar to the setup used in the current tests but with the following differences:

- Rectangular cross-sections instead of I-joists
- The gypsum board is provoked to fall-off after 45 min by a manual intervention, while in this test series, the fall-off occurred naturally.
- The test is terminated at 60 min, while in this test series, the tests were terminated based on the charring progression in each test.

The determination of PL for an insulation product is then based on the temperature of a TC at 100 mm depth at the intersection between the insulation and the rectangular beam at 45 and 60 min.

As the setup in this test series is not performed according to the test setup in prEN 1995-1-2, the results cannot be used as documentation for the PL level for the tested insulation products.

An adjustment of the test method for determination of the PL level should be considered for insulations used to protect I-joists, as the obtained recession rate is much lower than previously reported values found through the PL test method.

4.3. Effect of Having a Non-loaded Test Specimen

Compared to a real floor, the test specimen in these experiments were not loaded. It is, therefore, relevant to consider what effect the lack of any load had on the charring rate and the recession rate.

One typical behaviour of loaded test specimens is deflections in the structural members when their cross-section is reduced. Deflections might cause increased distance between structural members, which might cause openings of gypsum board joints and cause extra stress to the screws and the boards, which ultimately might fall off or crack.

For a deflection to occur, a significant reduction in the cross-section of the I-joist flanges must be present. In this paper, it is shown that several flanges were heavily charred already in the protected phase, i.e., while the gypsum board was in place. It is, therefore, likely that gypsum board failure would have occurred earlier if the test specimen had been loaded. However, Figures 10, 11 show that the calculated charring rate in the protected phase would not have been much different, although failure of the gypsum board had occurred slightly earlier.

After the failure of the gypsum boards, the increased distance between structural members would increase the probability that insulation falls down. Fall-down of insulation will further enhance the lateral charring, as explained in Sect. 4.2.3. However, the insulation in these tests stayed in general well in place, supported by the profile of the joist. This effect is believed to compensate for a small increased distance between the I-joists in case of a deflection.

Another effect that would have changed the failure time of the gypsum board is if the test specimen had been built with I-joists of one size. As an example, the small flanges in Test 2 and Test 3 had charred more than the screw length at the time of gypsum board failure. In those tests, it is evident that the gypsum board had failed earlier if I-joists with only small flanges were used.

5. Conclusions

The experiments were performed to develop data for improvement of the design methods in EN 1995-1-2.

The results from the experiments show that the charring rates for an I-joist with flanges of solid wood and Laminated Veneer Lumber are comparable.

The charring rates in the protected phase varied between 0.40 mm/min and 0.76 mm/min and the charring rate decreased with increasing flange size.

The charring rate during the post-protected phase varied from 0.54 mm/min to 1.72 mm/min. The uncertainty of the measurements was highest for the post-protected phase.

All charring rates of the I-joists in the protected phase were lower than the calculated values of rectangular cross-sections in EN 1995-1-2:2004. Compared to the new design method for I-joists in the final draft of prEN 1995-1-2:2021, there was a better match between experimental and calculated charring rates and the discrepancies were mainly on the conservative side.

The remaining cross-section area of all I-joist flanges had a trapezoid-like or rounded shape, which is characteristic of lateral charring.

Several flanges were heavily charred on the lateral side, although there was barely any post-protected phase. This highlights that lateral charring of the flanges of an I-joist can be significant in the protected phase.

Overall, the insulation stayed well in place after gypsum board fall-off. In most tests, the insulation was still in its place at the end of the test. This is due to the I-joist profile, which has a positive impact on keeping the insulation in its place. This advantage could be exploited in practical installation of insulation. All four insulation products showed a lower recession rate than typical values reported for glass wool insulation. The difference was more pronounced for the wood fibre and cellulose insulations. The recession rates were at the lower end of previously reported values for these types of insulation. The cellulose loose-fill insulation had the lowest recession rate at 1.1 mm/min, which is lower than any value reported previously for combustible insulations.

The low values found can possibly be explained by a different test setup and negligible shrinking of the insulation. Further, the recession rates in this test series were mainly measured in the protected phase, while reported values are often reported for the post-protected phase.

These tests have provided new knowledge on the topic I-joists and combustible insulations. Due to few repetitions of the experiments, results should be considered as indicative and should be completed with instrumented full-scale loaded tests.

Further research is needed on the following topics: Advanced analysis of the lateral charring, more insulation products to be investigated as evidently there are large differences between them, fall-down time and shrinkage of the insulations as these parameters directly affect the calculated recession rates and verification of test method for determining the protection levels for insulations for assemblies with I-joists.

Acknowledgements

The authors gratefully acknowledge the financial support by the Research Council of Norway, project no. 294649 and several partners through the Fire Research and Innovation Centre, www.fric.no. The research was partially supported by the Estonian Centre of Excellence in Zero Energy and Resource Efficient Smart Buildings and Districts, ZEBE (Grant No. 2014-2020.4.01.15-0016) funded by the European Regional Development Fund.

Funding

Open access funding provided by NTNU Norwegian University of Science and Technology (incl St. Olavs Hospital - Trondheim University Hospital).

Open Access This article is licensed under a Creative Commons Attribution 4.0 International License, which permits use, sharing, adaptation, distribution and reproduction in any medium or format, as long as you give appropriate credit to the original author(s) and the source, provide a link to the Creative Commons licence, and indicate if changes were made. The images or other third party material in this article are included in the article's Creative Commons licence, unless indicated otherwise in a credit line to the material. If material is not included in the article's Creative Commons licence and your intended use is not permitted by statutory regulation or exceeds the permitted use, you will need to obtain permission directly from the copyright holder. To view a copy of this licence, visit <http://creativecommons.org/licenses/by/4.0/>.

References

1. EN 1995-1-2:2004/AC:2009 (2004) Brussels, Belgium
2. National Forest Products Association (2018) National design specification for wood construction. A. W. Council, Worthing
3. LaMalva K, Hopkin D (2021) International handbook of structural fire engineering. Springer, Cham
4. Brandon D, Hopkin D, Emberley R, Wade C (2021) Timber structures. In: LaMalva K, Hopkin D (eds) International handbook of structural fire engineering Springer, Cham, pp 235–322
5. CSA O86:14 (R2019) Engineering design in wood, Canada
6. Friquin KL (2011) Material properties and external factors influencing the charring rate of solid wood and glue-laminated timber. *Fire Mater* 35(5):303
7. M. Klippel, J. Schmid, and A. Frangi, "Fire design of CLT. In: Proceedings of the Joint Conference of COST Actions FP1402 & FP1404 KTH Building Materials, Cross Laminated Timber—a Competitive Wood Product for Visionary and Fire Safe Buildings," in *Proceedings of the Joint Conference of COST Actions FP1402 & FP1404 KTH Building Materials, Cross Laminated Timber—a Competitive Wood Product for Visionary and Fire Safe Buildings*, 2016, pp. 101–122
8. EN 1991-1-2 (2002) Brussels, Belgium
9. ISO 834-1 (1999) Fire-resistance tests—elements of building construction—Part 1: general requirements, ISO
10. Östman B et al (2010) Fire safety in timber buildings—technical guideline for Europe. SP Rep 2010:19
11. AS/NZS 1720.4:2019 (2019) Timber structures—Part 4: Fire resistance of timber elements, Australia/New Zealand
12. Buchanan A, Östman B (2022) Fire safe use of wood in buildings: global design guide, 1st edn. CRC Press, Boca Raton
13. König J, Walleij L (2000) Timber frame assemblies exposed to standard and parametric fires. Part 2: a design model for standard fire exposure. Swedish Institute for Wood Technology Research, Stockholm
14. Just A (2010) Post protection behaviour of wooden wall and floor structures completely filled with glasswool. In 6th International conference on Structures in Fire, SiF Conferences

15. Östman B, König J, Schmid J, Just A (2012) Brandsäkra trähus 3: nordisk-baltisk kunskapsöversikt och vägledning. SP Rep 2012:18
16. Just A, Schmid J (2018) Improved fire design models for Timber Frame Assemblies—Guidance document. COST Action FP1404, Zürich
17. IMARC Group (2022) I-joist market: global industry trends, share, size, growth, opportunity and forecast 2023–2028. International Market Analysis Research and Consulting Group, Brooklyn
18. König J (2006) Fire exposed simply supported wooden I-joists in floor assemblies. SP Rep 2006:44
19. Hidalgo JP, Welch S, Torero JL (2015) Performance criteria for the fire safe use of thermal insulation in buildings. *Constr Build Mater* 100:285
20. Tiso M (2018) PhD-thesis: The contribution of cavity insulations to the load-bearing capacity of timber frame assemblies exposed to fire. Tallinn University of Technology, Tallinn
21. Tiso M, Just A (2018) Fire protection provided by insulation materials—a new design approach for timber frame assemblies. *Struct Eng Int* 27(2):231
22. Tiso M, Just A, Mäger KN (2016) Behavior of wooden based insulations at high temperatures. *Energy Procedia* 96:729
23. Tiso M, Just A (2017) Design criteria for insulation materials applied in timber frame assemblies. *J Struct Fire Eng* 9(3):252
24. Mäger KN, Tiso M, Just A (2020) Fire design model for timber frame assemblies with rectangular and i-shaped members. International scientific conference on wood & fire safety Springer, Cham
25. Mäger KN, Just A (2019) 52-16-1 Preliminary design model for wooden I-joists in Fire presented at the International Network on Timber Engineering Reserach (INTER) Meeting 52
26. Final draft of prEN 1995-1-2 (2021) Eurocode 5: design of timber structures Part 1–2: general-structural fire design
27. EN 1363-1:2020 (2020) Brussels, Belgium
28. Winter S, Werther N, Hoffmann V, Kammerer E, Rauch M (2019) Standardisierung der brandschutztechnischen Leistungsfähigkeit von Holztafelkonstruktionen mit biogenen Dämmstoffen. Technical University Munich (TUM), Munich
29. EN 520:2004 + A1:2009 (2004) Brussels, Belgium
30. EN 13171:2012 + A1:2015 (2012) Belgium, Brussels
31. EN 15101-1:2013 + A1:2019 (2013) Brussels, Belgium
32. EN 13166:2012 + A2:2016 (2012) Brussels, Belgium
33. IEC 60584-1:2013 (2013) Thermocouples—Part 1: EMF specifications and tolerances, IEC, Brussels
34. Fahrni R, Schmid J, Klippel M, Frangi A. (2018) Correct temperature measurements in fire exposed wood. In Proceedings of the 2018 World conference on timber engineering, World Conference on Timber Engineering (WCTE)
35. Pope I, Hidalgo JP, Hadden RM, Torero JL (2022) A simplified correction method for thermocouple disturbance errors in solids. *Int J Therm Sci* 172:107324
36. Beck JV (1962) Thermocouple temperature disturbances in low conductivity materials. *J Heat Transf* 84(2):124
37. Sultan MA (2008) Fire resistance of wood joist floor assemblies. *Fire Technol* 44(4):383
38. Kodur V, Stein J, Fike R, Tabbador M (2017) Comparative fire performance of traditional lumber and engineered wood joists. *J Struct Fire Eng* 8(1):2–13
39. Manguse H (2020) Master thesis: charring analysis of wooden I-joists in standard fire. Tallinn University of Technology, Tallinn

Publisher's Note Springer Nature remains neutral with regard to jurisdictional claims in published maps and institutional affiliations.